Tests of Modulated Intensity Small Angle Scattering in time of flight mode

G. Brandl[a,b], J. Lal[c], J. Carpenter[c,d], L. Crow[d], L. Robertson[d], R. Georgii[a,b], P. Böni[b], M. Bleuel[e]

[a]*Forschungsneutronenquelle Heinz Maier-Leibnitz, Technische Universität München, Lichtenbergstr. 1, 85747 Garching, Germany*
[b]*Physik Department E21, Technische Universität München, James-Franck-Str., 85747 Garching, Germany*
[c]*Argonne National Laboratory, Materials Science Division, Argonne, IL 60439, USA*
[d]*Oak Ridge National Laboratory, Oak Ridge, TN 37831-6477, USA*
[e]*Technical University of Delft, Mekelweg 15, 2629JB Delft, Netherlands*

Abstract

We report results of tests of the MISANS technique at the CG-1D beamline at High Flux Isotope Reactor (HFIR), Oak Ridge National Laboratory (ORNL). A chopper at 40 Hz simulated a pulsed neutron source at the beamline. A compact turn-key MISANS module operating with the pulsed beam was installed and a well characterised MnSi sample was tested. The feasibility of application of high magnetic fields at the sample position was also explored. These tests demonstrate the great potential of this technique, in particular for examining magnetic and depolarizing samples, under extreme sample environments at pulsed sources, such as the Spallation Neutron Source (SNS) or the planned European Spallation Source (ESS).

Keywords: MIEZE, spin echo, HFIR, MISANS, ESS

1. Introduction

MISANS, MIEZE (Modulation of Intensity with Zero Effort) in the Small Angle Neutron Scattering (SANS) geometry is a rather new technique to probe quasi-elastic scattering with extremely high energy resolution. The method is well understood [1, 2, 3] and efforts are under way [4, 5] to establish the technique as a standard tool for measurements of slow dynamics.

The general trend of new neutron sources to be accelerator driven and thus to provide pulsed neutron beams raises the question how MISANS will perform in a pulsed mode. In earlier experiments the feasibility of MISANS on pulsed sources was demonstrated [6, 7], however these tests were only using the direct beam and relative low MIEZE frequencies.

The goal of this experiment was to show that a MIEZE can be set up easily at a new beamline and works well in the time-of-flight mode with samples. Therefore a compact turn-key MISANS setup from the FRM II in Munich [4] was installed at the HFIR in Oak Ridge, Tennessee, USA, at the beamline CG-1D [8].

2. Setup of the Experiment

The used setup is shown in Figure 1: Two sets of MIEZE coils inside μ-metal shielding [9, 4] are placed between two polarizers. The polarizers are polarising solid state benders [10], which polarise the transmitted beam, but keep the collimation intact [11]. We used two approximately $10 \times 10\,\mathrm{mm}^2$ apertures (A_1 and A_3 in Figure 1) in about 3 m distance from each other for a rough collimation and suppression of the reflected spin states from the polarizers. The frequencies in the RF coils ranged between 46 and 149 kHz and matched the static fields:

$$\omega = 2\pi \cdot f = \gamma B \quad \text{with} \quad \gamma = 2\pi \cdot 2.913\,\mathrm{kHz/G}. \qquad (1)$$

In order to simplify the setup, the coupling coils were replaced by small guide fields and therefore all static fields were either parallel or anti-parallel to the strong magnetisation fields of the polarizers. This simplification of the setup removed the need for an adiabatic rotation of the neutron polarisation in the static fields by 90° as usual in MIEZE experiments and thus al-

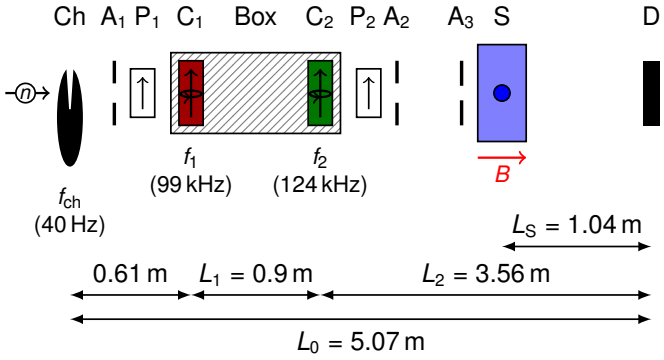

Figure 1: Sketch of the setup used for the MISANS experiment during the second beam session, viewed from the side. The chopper (Ch) provided a pulsed beam with a frequency of 40 Hz and a pulse length of 0.14 ms, corresponding to a chopper opening of 2°. The two polarizers (P_1 and P_2) were placed before and after the zero field region (hatched) of the MIEZE box, which contained the two MIEZE coils (C_1 and C_2). Three apertures (A_1 to A_3) were installed so that the beam is restricted to the sample (S), located inside a cryomagnet. The time-resolved detector (D) was placed at the correct distance to fulfill the MIEZE condition (eq. 3).

Email address: Robert.Georgii@frm2.tum.de (R. Georgii)

lowed a quicker adjustment of the setup in a new environment. The trade-off is that the MIEZE coils can only be operated in a $\pi/2$-mode, since the initial polarization is parallel to the static field of the B_0 coils. In this mode, each MIEZE coil must perform a $\pi/2$ flip to achieve the coherent splitting of two spin states that leads to the focused coherent overlap at the MIEZE point [12].

In contrast, in the usual MIEZE setup, which is preferred for all new developments, each MIEZE coil induces a π flip, and in combination with a "bootstrap" arrangement a factor of four in time resolution is gained in comparison to our $\pi/2$ mode setup.

For this time-of-flight MIEZE instrument, the RF amplitude needs to be modulated to match the condition

$$\gamma B \frac{l}{v} = \frac{\pi}{2} \quad \Rightarrow \quad B(\lambda) = \frac{\pi h}{2 m_n \gamma l} \frac{1}{\lambda}, \tag{2}$$

where h is Planck's constant, l is the RF coil thickness, v the neutron velocity, m_n its mass and λ its wavelength. In a time-of-flight instrument, the wavelength of a neutron with time of flight t at one component is given by $\lambda = ht/m_n x$, where x is the component's distance from the source. As the MIEZE module was originally developed for operation at a reactor source, the RF current was not modulated with the time of flight in the present setup.

As detector we used a circular multi-channel-plate prototype [13], with a diameter of 40 mm and only about 15–20 % detection efficiency for cold neutrons, but it provided sufficient time resolution and a very good spatial resolution (pixel size about 10 µm), both of which might become very useful in future tests at higher time resolution. The detector was always positioned according to the MIEZE condition

$$L_2 = \frac{L_1}{f_2/f_1 - 1}, \tag{3}$$

where L_1 is the distance between the coils, L_2 the distance between second coil and detector and f_i are the RF frequencies.

The chopper at CG-1D has an opening of 2° and was running at 40 Hz, which results in a pulse length of 0.14 ms. At the first MIEZE coil, positioned 0.6 m from the chopper, this amounts to a wavelength spread of $\Delta\lambda/\lambda \approx 15\,\%$ at $\lambda = 3.5$ Å and 8 % at $\lambda = 6.5$ Å. At the detector position at 5.07 m distance, the $\Delta\lambda/\lambda$ reduced to 1.7 % and 0.9 %, respectively.

3. Results

We report the results from two separate beam sessions, where we implemented slightly different instrumental parameters. The goal in the first beam session was to set up the MIEZE devices for the first time at CG-1D, while the goal in the second beam session was to perform a first sample measurement.

3.1. First session

Figure 2 shows the result of the first test, a MIEZE modulation on the time-of-flight spectrum of the chopped beam at CG-1D with two different frequencies. The absorption edges of

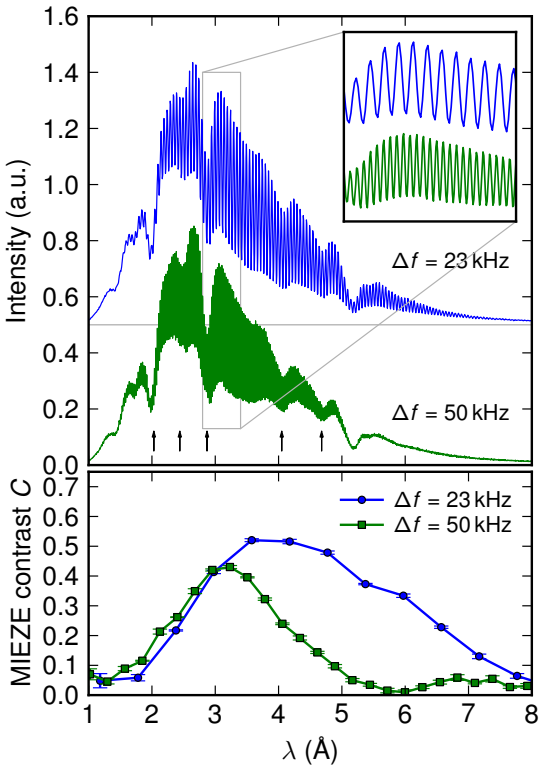

Figure 2: Intensity modulation and resulting contrast for the direct beam wavelength spectrum for two different MIEZE frequencies, $\Delta f = 23$ kHz and $\Delta f = 50$ kHz. The contrast is calculated by binning the spectrum into 8 bins per oscillation and fitting a sinusoidal signal to the summation of 12 individual oscillations for each point. The black arrows indicate the Bragg absorption edges of Al. Note that for better clarity, the spectrum for $\Delta f = 23$ kHz has been shifted by 0.5 on the intensity scale.

aluminum (marked with black arrows) and silicon (used in the solid-state polarizers) are clearly visible as dips in the Maxwellian shape of the spectra and were used to calibrate the time-of-flight to wavelength conversion. The RF frequencies were 46/69 kHz and 99/149 kHz, respectively, with distances $L_1 = 0.9$ m and $L_2 = 1.8$ m to fulfill the MIEZE condition. For calculating the MIEZE contrast in these and all other spectra, the spectrum is binned into 8 bins per MIEZE oscillation. Each oscillation spans a time-of-flight interval $t = 1/\Delta f$. To improve statistics, 8 to 15 individual oscillations are summed before a sinusoidal signal

$$I(n) = B + A \sin\left(\frac{2\pi}{8} \cdot n + \varphi\right) \quad \text{with} \quad n = 1, \ldots, 8 \tag{4}$$

with a fixed phase φ is fitted to the spectra. The contrast A/B of the fitted signal is the MIEZE contrast. The maximum contrast in our tests was about 50 %, which is most likely due to one of the MIEZE-coil sets having been damaged during the oversea transport causing static stray fields near the RF-coils and therefore interfering with the correct operation of the flippers.

Note that for $\Delta f = 50$ kHz, the effect of not ramping the RF current becomes clearly visible: the $\pi/2$ flip is achieved for neutrons of 3 Å, which means that at the same current neutrons of 6 Å will be flipped by π, which makes the contrast vanish

completely in our MIEZE mode. If there was enough intensity at 9 Å, one should see a considerable contrast again, in this case making $3\pi/2$ flips in the coils.

3.2. Second session

All the following measurements were performed in a second beam time, using only one set of RF frequencies of 99/124 kHz. The frequency ratio was chosen differently because with eq. (3) it results in a longer distance between second coil and detector, and allowed us to insert a cryomagnet at the sample position.

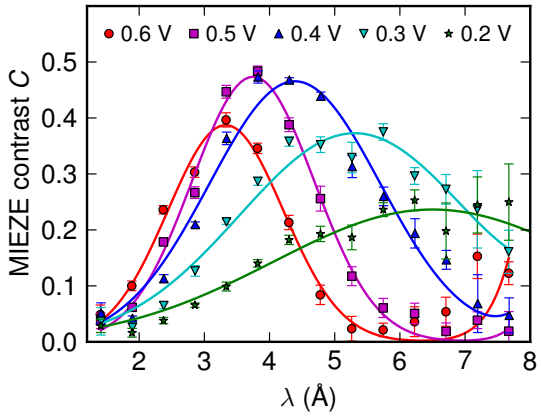

Figure 3: Contrast as a function of wavelength in the direct beam for various output voltages applied at the RF generator. The solid lines are guides to the eye. The MIEZE frequency was $\Delta f = 25$ kHz. Note that with eq. (2) half the RF field should flip twice the wavelength; this does not hold for the output voltage due to nonlinearities in the RF amplifier and circuit.

To elucidate the effect of RF current ramping, figure 3 shows the contrast as a function of wavelength in the direct beam for various output voltages in the RF generators. Note that on the one hand, towards very short wavelengths the initial beam polarization decreases rapidly, and therefore the maximum MIEZE contrast decreases. On the other hand, for large wavelengths the effect of stray fields becomes more pronounced, which again influences the maximum contrast.

Without changing the MIEZE setup we moved the detector 3 cm out of the direct beam in order to measure the neutrons scattered by the helical magnetic order in a MnSi sample placed inside the cryostat at zero field. MnSi is a weak itinerant ferromagnet that below $T_c = 28.9$ K forms a magnetic spiral with a pitch $d \sim 180$ Å, and magnetic satellite peaks become observable at $q = 2\pi/d = 0.035$ Å^{-1} in the $\langle 1\,1\,1\rangle$ directions [14]. We aligned the sample such that one of the peaks falls onto the detector in the small-angle scattering condition: see Figure 4. The vertical arrows on the plot are the calculated positions for the Bragg peak from the helical order using

$$q \approx \frac{2\pi}{\lambda}\sin(2\vartheta) \quad \Rightarrow \quad 2\vartheta \approx \sin^{-1}\left(\frac{qht}{2\pi m_n L_0}\right), \tag{5}$$

with the position of the sample peak $q = 0.035$ Å^{-1}, the Planck constant h, the neutron mass m_n, the time of flight t between the chopper and the detector for a distance $L_0 = 5.066$ m. The peak

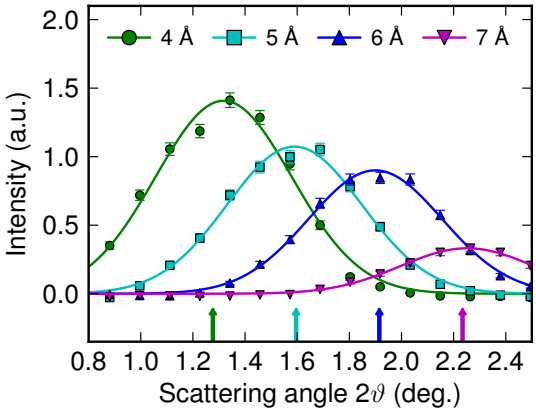

Figure 4: Intensity of the magnetic MnSi peaks as a function of position on the detector for various wavelengths. The detector was moved by 3 cm out of the direct beam for fulfilling the Bragg condition and the intensity was summed over 1Å intervals around the given wavelength. The vertical arrows represent a calculation of the expected Bragg positions of the MnSi peak for the mean wavelength of the interval.

intensity moves further away from the direct beam for longer neutron wavelengths in order to maintain Bragg's law.

For the data analysis, the part of the direct beam still visible on the detector has been subtracted in the form of a measurement at high temperatures, where no magnetic signal is present. The blue curve in Figure 5 shows the contrast measured in the neutron beam scattered by the MnSi sample at $T = 27.55$ K at the Bragg peak at $q = 0.035$ Å^{-1} for different spin-echo times, corresponding to different wavelengths in the incoming beam according to

$$\tau_{\mathrm{MIEZE}} = \frac{m_n^2}{h^2}\,\Delta f\, L_S\, \lambda^3, \tag{6}$$

with the sample–detector distance $L_S = 1.035$ m.

To obtain the intermediate scattering function $S(q,\tau)$, shown as the black curve in Figure 5, this data was normalized to the contrast measured analogously at $T = 2$ K (the green curve), serving as the reference measurement of the instrumental resolution [4]. It is expected that this $S(q,\tau)$ is equal to one, since the sample dynamics below T_c are too slow to be observed at the present time resolution at the Bragg peak [4, 15].

To finally assess the field compatibility of the technique beyond what had previously been demonstrated, we moved the detector back into the direct beam and looked at the contrast of the MIEZE signal as a function of a horizontal magnetic field at the sample position.

Figure 6 confirms that the MIEZE technique works with unshielded horizontal magnetic fields of up to 1 T. The observed drop in contrast to about 70 % of its zero-field value we attribute to the fact that we performed this experiment without coupling coils and with a low-quality μ-metal shielding around the MIEZE coils. Nevertheless the results show that MIEZE works even under unfavourable stray field conditions.

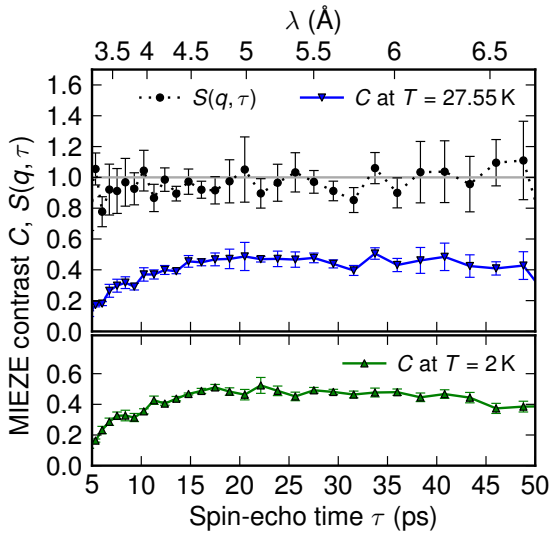

Figure 5: The intermediate scattering function $S(q,\tau)$ of the MIEZE signal from MnSi at $q = 0.035\,\text{Å}^{-1}$ is shown for $T = 27.55\,\text{K}$ as measured (blue) and after normalization (black) with the instrumental resolution function as determined at $T = 2\,\text{K}$ (green). The spin-echo times are calculated according to eq. (6).

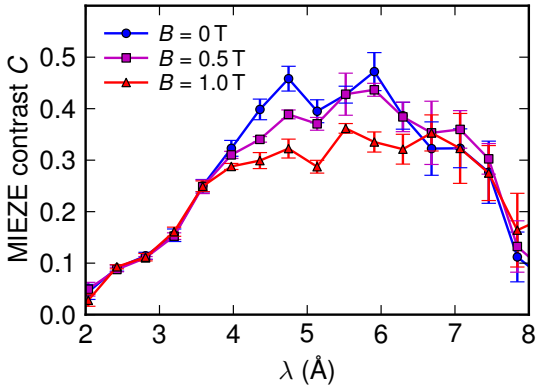

Figure 6: Contrast of the MIEZE signal in the direct beam for various magnetic fields at the sample position. The small loss of C with increasing field is due to the missing coupling coils and the insufficient μ-metal shielding.

4. Concluding Remarks

The effort to establish MISANS as a measurement technique for TOF applications is on the way and this paper documents important results along the path: the experiment establishes that MISANS can measure samples on pulsed neutron beamlines and the measurement of a MIEZE-signal in the direct beam with a 1 T horizontal field at the sample region demonstrates that this is a most promising technique for measurements of slow dynamics in high magnetic fields.

In the future, the setup could be extended to develop a MIEZE insert available as a standard option at several instruments at the SNS or at a dedicated MIEZE-SANS instrument at HFIR. It is also planned to propose a MISANS-type instrument for the European Spallation Source (ESS). Here, the instrument can benefit from the extended wavelength range, since the relaxed requirements on wavelength resolution typical for SANS are also acceptable for MIEZE-SANS. This means that similar gain factors can be expected.

5. Acknowledgements

We acknowledge the support of Ian S. Anderson for making these tests possible at HFIR. We are grateful for the help of Mike Fleenor and the staff at HFIR during the beam times. We also acknowledge very helpful discussions with Wolfgang Häußler and the technical support of Reinhard Schwikowski at the FRM II.

This work was funded by ONRL, the U.S. Department of Energy, BES-Materials Science, under Contract DE-AC02-06-CH117, and by the German BMBF under "Mitwirkung der Zentren der Helmholtz Gemeinschaft und der Technischen Universität München an der Design-Update Phase der ESS, Förderkennzeichen 05E10WO1."

References

[1] R. Gähler, R. Golub, T. Keller, Possible improvements in high resolution spectroscopy, Physica B: Condensed Matter 156-157 (1989) 653 – 656, ISSN 0921-4526, doi:10.1016/0921-4526(89)90754-0.

[2] P. Hank, W. Besenböck, R. Gähler, M. Köppe, Zero-field neutron spin echo techniques for incoherent scattering, Physica B: Condensed Matter 234-236 (1997) 1130 – 1132, doi:10.1016/S0921-4526(97)89269-1.

[3] T. Keller, Höchstauflösende Neutronenspektrometer auf Basis von Spinflippern – neue Varianten des Spinecho-Prinzips, Ph.D. thesis, Technische Universität München, 1993.

[4] R. Georgii, G. Brandl, N. Arend, W. Häußler, A. Tischendorf, C. Pfleiderer, P. Böni, J. Lal, Turn-key module for neutron scattering with sub-micro-eV resolution, Applied Physcis Letters 98 (2011) 073505, doi:10.1063/1.3556558.

[5] G. Brandl, R. Georgii, W. Häußler, S. Mühlbauer, P. Böni, Large scales–long times: Adding high energy resolution to SANS, Nuclear Instruments and Methods in Physics Research A 654 (2011) 394 – 398, doi:10.1016/j.nima.2011.07.003.

[6] M. Bleuel, M. Bröll, E. Lang, K. Littrell, R. Gähler, J. Lal, First tests of a MIEZE (modulated intensity by Zero effort)-type instrument on a pulsed neutron source, Physica B: Condensed Matter 371 (2) (2006) 297 – 301, ISSN 0921-4526, doi:10.1016/j.physb.2005.10.124.

[7] H. Hayashida, M. Kitaguchi, M. Hino, Y. Kawabata, R. Maruyama, T. Ebisawa, Development of a resonance spin flipper for NRSE/MIEZE on a pulsed neutron beam with an oscillating frequency of 500 kHz, Nuclear Instruments and Methods A 574 (2) (2007) 292 – 296, doi:10.1016/j.nima.2007.01.179.

[8] CG-1, Instrument Development Beam Line, URL `http://neutrons.ornl.gov/instruments/HFIR/CG1/`, 2010.

[9] N. Arend, R. Gähler, T. Keller, R. Georgii, T. Hils, P. Böni, Classical and quantum-mechanical picture of NRSE–measuring the longitudinal Stern-Gerlach effect by means of TOF methods, Physics Letters A 327 (1) (2004) 21 – 27, ISSN 0375-9601, doi:10.1016/j.physleta.2004.04.062.

[10] T. Krist, H. Fritzsche, F. Mezei, A large-angle neutron polarisation analyser, Applied Physics A 74 (2002) s221 – s223, doi:10.1007/s003390101093.

[11] M. Bleuel, E. Lang, T. Krist, W. Wagner, J. Lal, SANSPOL at a pulsed source, Physica B: Condensed Matter 397 (1-2) (2007) 85 – 87, doi:10.1016/j.physb.2007.02.044.

[12] T. Ebisawa, R. Maruyama, S. Tasaki, M. Hino, Y. Kawabata, D. Yamazaki, N. Torikai, K. Soyama, Neutron resonance spin echo methods for pulsed source, Nuclear Instruments and Methods A 529 (1-3) (2004) 28 – 33, doi:10.1016/j.nima.2004.04.171.

[13] A. Tremsin, J. Vallerga, J. McPhate, O. Siegmund, W. Feller, L. Crow, R. Cooper, On the possibility to image thermal and cold neutron with sub-15μm spatial resolution, Nuclear Instruments and Methods in Physics Research Section A: Accelerators, Spectrometers, Detectors and Associated Equipment 592 (3) (2008) 374 – 384, doi:10.1016/j.nima.2008.03.116.

[14] B. Lebech, P. Harris, J. S. Pedersen, K. Mortensen, C. I. Gregory, N. R. Bernhoeft, M. Jermy, S. A. Brown, Magnetic phase diagram of MnSi, J. Magn. Magn. Mater. 140-144 (1995) 119–120.

[15] C. Pappas, E. Lelièvre-Berna, P. Falus, P. M. Bentley, E. Moskvin, S. Grigoriev, P. Fouquet, B. Farago, Chiral Paramagnetic Skyrmion-like Phase in MnSi, Physical Review Letters 102 (19) (2009) 197202, doi: 10.1103/PhysRevLett.102.197202.